Contemporary Mathematics
Volume **469**, 2008

On the Estimation of Topological Entropy on Surfaces

S. Newhouse, M. Berz, J. Grote, and K. Makino

Dedicated to Misha Brin on the occasion of his sixtieth birthday.

ABSTRACT. We provide a rigorous lower bound for the topological entropy of planar diffeomorphisms in terms of the geometry of finite pieces of stable and unstable manifolds of hyperbolic periodic points. Our results suggest the possibility of writing computer programs which would automate the estimation of reasonable approximations for the topological entropy of mappings and differential equations. Applying them to the standard Henon map $H(x,y) = (1+y-ax^2, bx)$ with $a = 1.4,\ b = 0.3$ gives the lower bound $h_{top}(H) \geq 0.46469$.

CONTENTS

1. Introduction

The topological entropy $h(f)$ of a discrete dynamical system f is an important invariant which gives a quantitative measure of orbit complexity. There are several natural definitions of this invariant, but, except in special cases (e.g., symbolic systems) it is difficult to compute or estimate. In one-dimensional dynamics a number of techniques have been introduced to develop algorithms for the estimation of $h(f)$ (see [**6**], [**1**], [**30**]).

1991 *Mathematics Subject Classification.* Primary: 37B40, 37C05, 37C29, 37D10; Secondary: 37B10.
Key words and phrases. Hénon map, hyperbolic, stable manifold, topological entropy, trellis, Taylor models.

In the case of two dimensional diffeomorphisms several ad-hoc methods have been developed [**15**], [**7**], [**12**], [**36**] to identify various subsets which factor onto symbolic systems, and hence, give lower bounds on the topological entropy. A numerical scheme based on length growth was given in [**29**].

In Pieter Collins work [**10**], [**11**] certain sets called *trellises* which consist of pieces of stable and unstable manifolds are used to describe forcing orbits, periodic orbits, and lower bounds for the entropy in various isotopy classes of diffeomorphisms which fix certain sets of orbits.

In this paper, we apply methods for the rigorous computation of stable and unstable manifolds to the problem of estimating the topological entropy of invariant sets given by certain trellises. We will use these methods to estimate the entropy of the standard Henon map: $H(x,y) = (1+y-ax^2, bx)$ for $a = 1.4, b = 0.3$. We obtain the lower bound $h_{top}(H) \geq 0.46469$. To our knowledge, this estimate is the largest lower bound currently available for the entropy of this map. Even so, it will be clear that this estimate can be improved, and we do not touch the issue of how closely one can expect to approximate the true entropy. In addition, we mention that we only consider lower bounds. The question of finding upper bounds which get close to the real entropy is virtually wide open. There are general upper bounds due to Yomdin [**34**], but in most cases they are much greater than the true entropy.

2. Definition and properties of Topological Entropy

Let (X,d) be a compact metric space, and let $f : X \to X$ be a continuous self-map. Given a positive integer n, and a real number $\varepsilon > 0$, a subset E of X is called an (n,ε)-separated set in X if, for $x \neq y \in X$, there is a $j \in [0,n)$ such that $d(f^j x, f^j y) > \varepsilon$. The maximal cardinality of any $(n,\varepsilon)-$separated set is denoted $r(n,\varepsilon)$, and the quantity

$$h(f) = h_{top}(f) = \lim_{\varepsilon \to 0} \limsup_{n\to\infty} \frac{1}{n} log\ r(n,\varepsilon)$$

is called the *topological entropy* of f. Thus number is a measure of orbit complexity of the system (f,X). It enjoys many nice properties (see e.g. [**32**]). For instance,

(1) If f and g are topologically conjugate, then $h(f) = h(g)$,
(2) If $f = g^n$ for some positive integer n, then, $h(f) = nh(g)$, and, if $\mathcal{M}(f)$ denotes the set of $f-$invariant probability measures of f, then
(3)
$$h(f) = \sup_{\mu \in \mathcal{M}(f)} h_\mu(f)$$
where $h_\mu(f)$ denotes the measure-theoretic entropy of f with respect to the measure μ.

In the case of smooth systems, the topological entropy is related to certain other geometric quantities.

Let $f : M \to M$ be a C^r diffeomorphism of a compact two dimensional C^r Riemannian manifold for $r \geq 1$. Given a C^r curve γ in M, let $|\,\gamma\,|$ denote the arclength of γ. Let $\log^+(x) = max(\log(x), 0)$ denote the positive part of the natural logarithm function. The length growth of γ is the quantity

$$G(\gamma) = G(\gamma, f) = \limsup_{n\to\infty} \frac{1}{n} \log^+ |\, f^n \circ \gamma\,|. \tag{1}$$

For $1 \leq r < \infty$, let $\mathcal{D}^r(M)$ denote the space of C^r diffeomorphisms of M with the uniform C^r topology. In the case $r = \infty$, the topology in $\mathcal{D}^\infty(M)$ is defined to be the weakest topology making all of the inclusions $\mathcal{D}^\infty(M) \to \mathcal{D}^r(M)$, $1 \leq r < \infty$, continuous.

THEOREM 2.1. **[28],[33]** *Let M be a compact C^∞ two dimensional manifold. and $f \in \mathcal{D}^\infty(M)$. Then,*

$$h_{top}(f) = \max_{curves\ \gamma} G(\gamma, f). \tag{2}$$

Further, the map $f \to h_{top}(f)$ is continuous as a map from the space of $\mathcal{D}^\infty(M)$ to **R**.

REMARK 2.2.
(1) We remark that, in higher dimensional manifolds the map $f \to h_{top}(M)$ from $\mathcal{D}^\infty(M) \to \mathbf{R}$ is not always continuous, although it is upersemicontinuous.
(2) For simplicity, Theorem 2.1 is stated for compact manifolds, and, hence, does not apply directly in the non-compact case. In our applications, which deal with $M = \mathbf{R}^2$, the Euclidean plane, all entropies will be on invariant compact subsets. So, we can and will use curves whose orbits stay in compact subsets to estimate entropy. For more precise statements on this topic, see [**27**].

There is a useful class of dynamical systems in which topological entropy is natural and computable. This is the class of *subshifts of finite type* or *topological Markov chains*. For ease of notation, frequently one uses the acronym *SFT* for subshifts of finite type, both singular and plural.

We will only need the case of automorphisms.

Let us recall the definition.

Let $J = \{1, 2, \ldots, N\}$ be a finite set of integers, and let Σ_N denote the set of doubly infinite sequences $\mathbf{a} = (\ldots, a_{-1}a_0a_1\ldots)$ of elements in J with the metric

$$d(\mathbf{a}, \mathbf{b}) = \sum_{i \in \mathbf{Z}} \frac{|\, a_i - b_i \,|}{2^{|\, i \,|}}.$$

The pair (Σ_N, d) is then a compact zero dimensional metric space. Let $\sigma : \Sigma_N \to \Sigma_N$ be the left shift automorphism defined by

$$\sigma(\mathbf{a})_i = \mathbf{a}_{i+1}$$

for all $i \in \mathbf{Z}$. This is a homeomorphism of Σ_N.

Given an $N \times N$ matrix whose entries are 0's and 1's, we define

$$\Sigma_A = \{\mathbf{a} \in \Sigma_N : A_{a_i a_{i+1}} = 1 \ \ \forall i\}$$

This is a closed subset of Σ_N which is invariant under σ. The pair (σ, Σ_A) is called a *subshift of finite type* or *topological Markov chain*.

The topological entropy of the pair (σ, Σ_A) is well-known to be the growth rate of the number of admissible $n-$blocks and is also equal to the logarithm of the spectral radius of A.

Given a smooth diffeomorphism (f, M), a *subsystem* of (f, M) is a pair (f, Λ) where Λ is a compact subset of M such that $f(\Lambda) = \Lambda$. A *subshift* of (f, M) is a subsystem (f, Λ) of (f, M) with the property that (f, Λ) is topologically conjugate to a subshift of finite type. We frequently abuse the notation by saying that a subset Λ of M is a subshift when the pair (f, Λ) is known. We also often say that Λ is a subshift of f.

A given smooth system may or may not have subshifts. The following remarkable theorem due to A. Katok shows that, in dimension two, a smooth system has subshifts if and only if it has positive topological entropy.

THEOREM 2.3. *(Katok* [**16**], [**20**]*) Let $r \geq 2$. A C^r diffeomorphism of a compact surface has positive topological entropy if and only if it possesses subshifts. In fact, if $h_{top}(f) > 0$ and $\varepsilon > 0$ is arbitrary, then there is a subshift Λ of f such that*

$$h_{top}(f,\Lambda) > h_{top}(f) - \varepsilon$$

Thus, in the case of surface diffeomorphisms f, it order to estimate the topological entropy, one only has to find subshifts with large entropy. The difficulty here is that these are often hard to find. In fact, one of our main purposes in this paper is to give methods to find subshifts whose entropies are close to that of f.

3. Trellises and Entropy

Let $r \geq 2$, and consider a C^r diffeomorphism f on the smooth connected two-dimensional manifold M.

Let $P = \{p_1, p_2, \ldots, p_k\}$ be a sequence of hyperbolic periodic points of f with associated stable and unstable manifolds $W^u(p_i), W^s(p_i)$. We recall that these are injectively immersed curves which are defined by

$$W^s(p_i) = \{y \in M : dist(f^n y, f^n p_i) \to 0 \text{ as } n \to \infty\},$$

$$W^u(p_i) = \{y \in M : dist(f^n y, f^n p_i) \to 0 \text{ as } n \to -\infty\}.$$

An *interval* in $W^u(p)(W^s(p))$ (or an *arc*) is a connected subset of $W^u(p)(W^s(p))$ which contains at least two points. An open interval will be written as (p,q) where p and q lie in the same connected subset of some $W^s(p)$ or $W^u(p)$. The boundary of (p,q) consists of the two element set $\{p,q\}$. We will denote the closure of a set E by $Cl(E)$, and the boundary of E by ∂E which is defined to be $Cl(E) \setminus interior(E)$. In the case of subsets of a stable and unstable manifold, we use the topology induced by the intervals.

A *trellis* $T = (\mathcal{U}, \mathcal{S})$ associated to the sequence P is a pair with the following properties.

(1) $\mathcal{U} = \{U_1, \ldots, U_k\}$ is a collection of compact intervals in $\bigcup_i W^u(p_i)$ whose union is backward invariant; i.e. $f^{-1}(\bigcup_i U_i) \subset \bigcup_i U_i$, and
(2) $\mathcal{S} = \{S_1, \ldots, S_k\}$ is a collection of compact intervals in $\bigcup_i W^s(p_i)$ whose union is forward invariant; i.e., $f(\bigcup_i S_i) \subset \bigcup_i S_i$.

Given a trellis $T = (\mathcal{U}, \mathcal{S})$, we let $U = \bigcup_i U_i$, $S = \bigcup_i S_i$ denote the union of the elements of the collections $\mathcal{U}, \mathcal{S}$, respectively. Abusing the language somewhat, we sometimes identify the collections $\mathcal{U}, \mathcal{S}$ with their unions, and speak of the trellis $T = (U,S)$ where U, S are subsets of M. Thus, the third condition of the definition of trellis (U,S) says that S is forward invariant and U is backward invariant.

Also, we use the standard notation for images $f^i(\mathcal{A})$ of collections of sets as $f^i(\{A\}) = \{f^i(A)\}$. In this way, we see that if T is a trellis, then so is each iterate $f^i(T)$ with $i \in \mathbf{Z}$.

We will only consider trellises for which $S \bigcap U \neq \emptyset$. Thus, the elements in $S \bigcap U$ are either periodic orbits or homoclinic points.

Throughout this paper, for simplicity, we assume that all trellises considered consist of pieces of stable and unstable manifolds of a single hyperbolic fixed point p_0. Generalizations to the case of arbitrary collections of periodic points are straightforward and will

be left to the reader. We also assume that the stable and unstable curves of the trellis have at most finitely many intersections. These intersections consist of transverse intersections and, perhaps, some homoclinic tangencies.

We let $HP = HP(T)$ denote the union of $\{p_0\}$ and the set of homoclinic points in $U \bigcap S$. We assume that there is at least one homoclinic point.

Next, we define a *homoclinic disk* R associated to T. This is a connected component of the complement $M \setminus (S \bigcup U)$ whose closure is homeomorphic to a compact topological 2-disk. Note that homoclinic disks are open subsets of M whose boundaries are piecewise smooth Jordan curves.

The boundary of $Cl(R)$ consists of stable and unstable arcs and the points in $HP \bigcap Cl(R)$.

We define the *stable boundary* of R to be the closure of the union of the stable arcs in ∂R, and the *unstable boundary* of R to be the closure of the union of the unstable arcs in ∂R. We denote these by $\partial^s R$, and $\partial^u R$, respectively. Each point p_i in $\partial R \bigcap HP$ will be called a *vertex* of R.

If all the vertices of ∂R are transverse, then the stable and unstable boundary arcs alternate as one moves along ∂R.

Of special importance to us will be homoclinic disks with exactly 4 transverse vertices. These will be called *rectangles*. Given such a rectangle, we order its vertices as (p_1, p_2, p_3, p_4) with $(p_i, p_{i+1}) \subset S$ or $(p_i, p_{i+1}) \subset U$ for $1 \leq i < 4$, and we write $R = R(p_1, p_2, p_3, p_4)$. On any surface M except the two-sphere S^2 this representation of rectangles is unique up to cyclic permutation of the vertices (since the complement of a disk is not a disk and our rectangles are assumed to be topological disks). In S^2, each such 4-tuple in HP gives rise to two disjoint (open) rectangles.

The stable boundary of a rectangle R consists of two maximal stable arcs which we call the *stable boundary components* of R. Similarly, the unstable boundary R consists of two maximal unstable arcs which we call the *unstable boundary components* of R.

Since f is a diffeomorphism and the stable and unstable manifolds are $f-$invariant, the following proposition is easily proved.

PROPOSITION 3.1. *If R is a rectangle associated to the trellis T, then, for any integer n, $f^n(R)$ is a rectangle associated to the trellis $f^n(T)$.*

Note that we can parametrize a rectangle R by choosing a homeomorphism h from the unit square $I^2 = [0,1] \times [0,1]$ onto $Cl(R)$ such that $h([0,1] \times \{0,1\}) = \partial^u R$ and $h(\{0,1\} \times [0,1]) = \partial^s R$. Fixing such a parametrization when it is desirable, we will refer to the unstable boundary components as the *top and bottom* boundary curves of R and the stable boundary components as the *left and right* boundary curves of R.

Now, let R be a rectangle.

A *full-height arc* in R is an embedding $\gamma : [0,1] \to Cl(R)$ such that $\gamma(0)$ and $\gamma(1)$ are in different unstable boundary curves of R and $\gamma(t) \in R$ for each $0 < t < 1$. Similarly, a *full-width arc* in R is an embedding $\gamma : [0,1] \to Cl(R)$ such that $\gamma(0)$ and $\gamma(1)$ are in different stable boundary curves of R and $\gamma(t) \in R$ for each $0 < t < 1$. As usual, we will often suppress the parametrizations of curves and identify the curve with its image.

An $s-disk$ in R is a homoclinic disk R_1 such that

(1) $R_1 \subset R$,
(2) $\partial^u R_1 \subset \partial^u R$, and
(3) $\partial^s R_1$ has a non-empty intersection with *both* unstable boundary components of R.

Similarly, a $u-disk$ in R is a homoclinic disk R_1 such that

(1) $R_1 \subset R$,
(2) $\partial^s R_1 \subset \partial^s R$, and
(3) $\partial^u R_1$ has a non-empty intersection with *both* stable boundary components of R.

Following the notation of Pieter Collins [**10**], let us call a bounded connected component of the complement of $S \bigcup T$ a *bigon* if it is a topological disk whose boundary contains exactly two (transverse) homoclinic points.

Now, let R_1 be an $s-$disk in R. Since R_1 is an open planar disk whose closure is a closed topological disk and only its stable boundary arcs can intersect R, it follows that there are exactly two stable boundary arcs of R_1 which are full-height arcs in R. Let us call these the *left* and *right* edges of R_1, and denote them by γ_l^s, γ_r^s. Further, each stable boundary curve of R_1 different from γ_l^s and γ_r^s has both of its endpoints in the same unstable boundary curve of R. Thus, we may think of R_1 as a full-height subrectangle of R in which certain open bigons may have been removed. The stable boundaries of these removed disks (if they exist) are smooth open arcs whose boundaries lie in the unstable boundary of R. A similar statement holds for $u-$disks.

See Figure 1 for examples.

Next, we define a relation $\rightarrow$ on a collection of disjoint rectangles analogous to the relation used in the construction of Markov Partitions in hyperbolic dynamics.

Let $\mathcal{R} = \{R_1, R_2, \ldots, R_s\}$ be a disjoint collection of rectangles associated to the trellis $T = (S,U)$.

The relation $\rightarrow$ on $\mathcal{R}$ is defined by saying that $R_i \rightarrow R_j$ if $R_i \bigcap f^{-1} R_j$ contains an $s-$disk D such that $f(D)$ is a $u-$disk in $f(R_i) \bigcap R_j$.

LEMMA 3.2. *Let R_i and R_j be two rectangles as above with the property that $R_i \rightarrow R_j$, and let γ be any full-width open arc in R_i. Then, there is an open subarc η of γ such that $f(\eta)$ is a full-width open arc in R_j.*

Remark. Lemma 3.2, which is fundamental for our work here, is in spirit related to results in Burns and Weiss [**7**], specifically, in regard to the techniques and applications of Lemmas 2.5 and 2.6 in [**7**]. However, the rectangles considered in [**7**] are compact and disjoint, and, hence, Burns and Weiss only need the sets $A_r(\alpha)$ on page 103 of [**7**] to be non-empty. In our work, at present, it seems that we need the corresponding sets to have non-empty interiors which originate in full height disks and map by an appropriate power of f to full-width disks.

Proof. Let R_{i1} be the $s-$disk in R_i which maps to a $u-$disk in R_j. The stable arcs in ∂R_{i1} break into two collections: those which are mapped by f into $\partial_{left} R_j$ and those which are mapped by f into $\partial_{right} R_j$. Let us call these collections $\mathcal{S}_{left}$ and $\mathcal{S}_{right}$, and their unions S_{left}, S_{right}, respectively. As we mentioned above, there are unique full-height stable boundary curves of R_{i1}: $\gamma_l^s \in \mathcal{S}_{left}$, $\gamma_r^s \in \mathcal{S}_{right}$.

The full-width curve γ meets both S_{left} and S_{right}. Letting $\phi : [0,1] \rightarrow \gamma$ be a parametrization of γ with $\phi(0) \in \partial_{left} R_i$ and $\phi(1) \in \partial_{right} R_i$, we set

$$t_0 = \sup_{t \in [0,1]} \phi(t) \in S_{left}.$$

Since $\phi(1) \in \partial_{right} R_i$, there must exist real numbers t' such that $t_0 < t' < 1$ and $\phi(t') \in S_{right}$.

Letting

$$t_1 = \inf_{t \in [t_0,1]} \phi(t) \in S_{right},$$

we obviously have $t_0 < t_1$. So, if we set ζ to be the restriction of ϕ to the open interval (t_0, t_1), then the image of ζ is the desired open subarc η of γ. QED.

Now, the collection of rectangles $\mathcal{R} = \{R_1, R_2, \ldots, R_s\}$ and the relation $\rightarrow$ determine an $s \times s$ incidence matrix as usual setting

$$A_{ij} = 1 \text{ iff } R_i \rightarrow R_j.$$

This in turn determines a subshift of finite type (σ, Σ_A) by

$$\Sigma_A = \{\mathbf{a} = (\ldots a_{-1}a_0a_1\ldots) : A_{a_i a_{i+1}} = 1 \ \forall i \in \mathbf{Z}\},$$

and $\sigma(\mathbf{a})(i) = \mathbf{a}(i+1)$ for all i.

Our main result here is the following.

THEOREM 3.3. *Suppose f is a C^∞ diffeomorphism of the C^∞ two dimensional manifold M such that one can find a trellis $T = (S,U)$ with associated collection $\mathcal{R}$ of rectangles with the relation $\rightarrow$ defined above and the associated subshift of finite type (σ, Σ_A). Then,*

$$h_{top}(f) \geq \log sp(A) \tag{3}$$

where $sp(A)$ is the spectral radius of A

Remark. We expect that this theorem holds under weaker smoothness assumptions, even for C^1 diffeomorphisms f. However, because our rectangles are not necessarily disjoint, a proof in this more general situation seems more technical and we have not attempted to seriously pursue that.

Proof.

It is well-known that

$$\log sp(A) = \limsup_{n\to\infty} \frac{1}{n} \log card(B_n) \tag{4}$$

where B_n is the set of distinct $n-$blocks in Σ_A.

Here an *$n-$block* $B_{j_0,j_1,\ldots,j_{n-1}}$ in Σ_A is a finite sequence $[j_0, j_1, \ldots, j_{n-1}]$ with the property that there is an element $\mathbf{a} = (\ldots a_{-1}a_0a_1\ldots) \in \Sigma_A$ such that $a_k = j_k$ for each $0 \leq k < n$.

We will make use of formula 2. Thus, it suffices to find a curve γ and a constant $C > 0$ such that, for all $n > 0$,

$$| f^{n-1}(\gamma) | \geq C \cdot card\ B_n. \tag{5}$$

Consider the collection of rectangles

$$\mathcal{R} = \{R_1, R_2, \ldots, R_s\}$$

as above.

Since the rectangles R_i are disjoint, they form a partition of the the union $\bigcup_i R_i$.

Let

$$\mathcal{R}^n = \bigvee_{i=0}^{n-1} f^{-i}\mathcal{R}$$

as usual.

The $n-$blocks are in one-to-one correspondence with the elements of the partition $\mathcal{R}^n$. Thus, it suffices to estimate the number of elements in the partition $\mathcal{R}^n$.

Since there are only s rectangles in our collection, it suffices to consider all elements

$$D_{i_0 i_1 \ldots i_{n-1}} = R_{i_0} \bigcap f^{-1} R_{i_1} \bigcap \ldots \bigcap f^{-n+1} R_{i_{n-1}}$$

with R_{i_0} a fixed element in $\mathcal{R}$.

Fix the element $D = D_{i_0 i_1 \ldots i_{n-1}}$, and let γ_{i_0} be a full-width open arc in R_{i_0}.

By Lemma 3.2 there is a subarc γ_{i_0,i_1} of γ_{i_0} such that $f(\gamma_{i_0 i_1})$ is a full-width arc in R_{i_1}.

Similarly, there is a subarc $\eta_{i_0 i_1}$ of $f(\gamma_{i_0 i_1})$ such that $f(\eta_{i_0 i_1})$ is a full-width arc in R_{i_2}.

The pull-back $\gamma_{i_0 i_1 i_2} = f^{-1}\eta_{i_0 i_1}$ is then a subarc of $\gamma_{i_0} \bigcap R_{i_0} \bigcap f^{-1} R_{i_1} \bigcap f^{-2} R_{i_2}$ which maps by f^2 to a full-width arc in R_{i_2}.

Continuing by induction, we obtain a subarc $\gamma_{i_0 i_1 \ldots i_{n-1}}$ of $\gamma_{i_0} \bigcap D$ such that

(1) for each $0 \leq j < n$, the image $f^j(\gamma_{i_0 i_1 \ldots i_{n-1}})$ is contained in R_{i_j}, and

(2) the image $f^{n-1}(\gamma_{i_0 i_1 \ldots i_{n-1}})$ is a full-width arc in $R_{i_{n-1}}$.

Moreover, since the rectangles $R_i's$ are disjoint (recall that they are open), we have that distinct elements $D_{i_0 i_1 \ldots i_{n-1}}$ give rise to disjoint arcs $\gamma_{i_0 i_1 \ldots i_{n-1}}$.

Letting C denote the minimum lengths of full-width arcs among the rectangles R_i, we get 5 as required. QED.

REMARK 3.4. The construction above has a familiar graph theory interpretation. Let Γ be the graph whose vertices are the indices $\{1, \ldots, s\}$ of the rectangles R_i with a directed edge e_{ij} from i to j if and only if $R_i \to R_j$. The matrix A is, by definition, the *incidence matrix* of the graph Γ. In this case, for each pair (i, j) there is at most one edge from i to j.

REMARK 3.5. **(The edge construction)** It is common to consider graphs with many edges joining a pair of vertices. For instance, suppose that Γ_1 is a graph with the vertices $\{1, \ldots, s\}$ and $k_{ij} \geq 0$ edges from i to j. In that case we consider the matrix $B = (B_{ij})$ defined by $B_{ij} = k_{ij}$. If we consider the new graph Γ_B whose vertices are the edges of Γ_1 and whose edges are the pairs $(e_{i_1 j_1}, e_{i_2 j_2})$ such that $j_1 = i_2$, then we get a new incidence matrix A_1 and, as is well-known, the spectral radius of A_1 is the same as that of B. This construction, which we will call the *edge* construction, corresponds in the case of trellises to the situation in which $R_i \bigcap f^{-1}(R_j)$ may consist of several disjoint $s-$disks in R_i, and $f(R_i) \bigcap R_j$ may, correspondingly, consist of several different $u-$disks in R_j. The corresponding matrix B which is non-negative integer valued, may be used to give a lower bound for the topological entropy of an invariant subset of f just as well. In our application of trellises to the the Henon maps below, we will make use of this construction.

4. Computing stable and unstable manifolds

The is a substantial literature dealing with algorithms for the computation of stable and unstable manifolds of a hyperbolic fixed point. For instance, we refer to the papers Francescini-Russo [**13**], Hubbard [**19**], Zou-Kostelich-Yorke [**35**], D. Hobson [**18**], Krauskopf and Osinga [**21**], and Cabré, Fontich, and de la LLave [**9**]. Most of these algorithms yield good results for fairly short pieces of the manifolds near the fixed point, but they deteriorate fairly quickly as one gets longer and longer pieces. Accordingly one important aspect of our work has been to develop adaptive verified methods for the computation of stable and unstable manifolds. This is done using Taylor Models and the computer program COSY INFINITY [**3**] which can be used to give rigorous error estimates of long parts of stable and unstable manifolds. In fact, current work on the implementation of *arbitrary precision arithmetic* in COSY INFINITY holds the promise of allowing one to compute extremely long pieces of invariant manifolds.

While the rigorous justification below of our estimate of topological entropy for the Henon map currently depends on the use of COSY INFINITY, it is possible to motivate the constructions using other, less accurate (in the large) computational methods. For this purpose, we will make use of the following theorem which combines ideas in [**19**] and [**9**].

THEOREM 4.1. *Let f be a C^r diffeomorphism from $\mathbf{R}^N \to \mathbf{R}^N$, $r \geq 1$, with a hyperbolic fixed point at p and associated splitting $T_pM = E^s \oplus E^u$ with dim $E^u = 1$. Let λ be the eigenvalue of $Df(p)$ with $|\lambda| > 1$, and let v be an associated eigenvector. For each $n \geq 1$ define the function $\gamma_n(t) = f^n(p + \lambda^{-n} tv)$. Then, the sequence of functions $\gamma_n(t)$ converges uniformly on compact sets to a C^r function $\gamma : E^u \to \mathbf{R}^N$ such that $\gamma(0) = 0$, $\gamma'(0) = v$, and*

$$f \circ \gamma(t) = \gamma(\lambda t) \tag{6}$$

for all real t.
The image $\gamma(E^u)$ coincides with the unstable manifold of p.

Remark. The results in [**9**] are much more general than Theorem 4.1. Also, Hubbard considers only analytic functions. He also considers multidimensional unstable manifolds, has many nice examples, and emphasizes the global nature of the parametrizing function γ.

5. Computation of the stable and unstable manifolds in Hénon Maps

We wish to apply our trellis theorem above to obtain a lower bound for the topological entropy of certain Henon maps.

Consider the Hénon family of maps

$$H(x,y) = (1 + y - a * x^2, b * x) \tag{7}$$

Letting $r = \sqrt{b^2 - 2b + 4a + 1}$, and allowing x, y to possibly be complex, it can be verified that the map H has two fixed points q_0, p_0 with

$$q_0 = (-\frac{r - b + 1}{2a}, -b\frac{r - b + 1}{2a}) \tag{8}$$

and

$$p_0 = (\frac{r + b - 1}{2a}, b\frac{r + b - 1}{2a}) \tag{9}$$

We now fix the parameters $a = 1.4,\ b = 0.3$ which are, in fact, the original parameters considered by Hénon in [**17**].

In this case the fixed points q_0, p_0 are both real hyperbolic saddle points.

We will focus on the right fixed point $p_0 \sim (0.6313544770895, 0.18940634312685)$ and consider a trellis associated to it.

This trellis will be constructed in two steps.

First, we construct a disjoint collection of 13 open rectangles $\mathcal{R} = \{R_1, R_1, \ldots, R_{13}\}$ bounded by pieces of the stable and unstable manifolds of p_0, and we consider the first return map to the union $\bigcup_j R_j$. Thus, we set $D = \bigcup_j R_j$, and, for $x \in D$, we define $r(x)$ to be the smallest positive integer such that $H^{r(x)}(x) \in D$. It turns out that the function $r(x) \geq 2$, and is constant on each R_i. We let $r_i = r(x)$ for $x \in R_i$. It also will turn out

that, for each pair i, j, either $R_i \bigcap H^{-r_i}(R_j)$ is empty or it consists of one or more full-height subrectangles, each of which maps by H^{r_i} to a full-width subrectangle in R_j. This gives us a 13×13 matrix A whose entries are non-negative integers, and a 13 dimensional vector $r = (2,2,2,2,5,5,6,5,2,2,6,7,6)$ of first return times. From this, in a more or less standard way, we build a tower, adding the new rectangles $R_{i,1} = H(R_i), R_{i,2} = H^2(R_i), \ldots, R_{i,r_i-1} = H^{r_i-1}(R_i)$ for each i. Taking the boundaries of the original rectangles and the new ones gives us a trellis with associated matrix B such that the logarithm of the spectral radius of B is (up to a standard numerical eigenvalue calculation) approximately 0.4646992601904559. Taking into account round-off errors in the eigenvalue computation, we can conservatively use 0.46469 as a lower bound for this spectral radius.

The matrix B has non-negative integer entries. The edge construction we described in Remark 3.5 at the end of section 3 gives a larger 0-1 matrix which can be used as in Theorem 3.3 to give give the following theorem.

THEOREM 5.1. *The topological entropy $h_{top}(H)$ of the Henon map*

$$H(x,y) = (1 + y - 1.4\, x^2,\ 0.3\, x)$$

satisfies the estimate

$$h_{top}(H) \geq 0.46469 \tag{10}$$

The proof of the theorem is computer assisted and based on the ability to rigorously enclose sufficiently long pieces of the stable and unstable manifolds in a tight enough manner. The details of the methods to obtain these enclosures and why they are rigorously satisfied under standardized requirements on computer arithmetic will be given elsewhere, but the key ideas will be discussed in section 6 below.

In the remaining part of the present section, we give a geometric desciption of the rectangles R_i and their mapping properties.

Let us first remark that it is not easy to find the rectangles we are about to describe. They were obtained by numerical experimentation. To enable the interested reader to repeat the numerical constructions, we describe them in some detail (without proof) in section 7.

Consider the right fixed point $p_0 \approx (.6313544770895048, .1894063431268514)$. There is a transverse homoclinic point $q_1 \approx (0.3388525493895907, -0.2551126297830196)$ which lies below p_0. We consider the arcs $S_1 \subset W^s(p_0)$ and $U_1 \subset W^u(p_0)$ forming a bigon D_0 whose vertices are p_0 and q_1. We call D_0 the *primary region* for H.

It turns out the every bounded orbit of H which is disjoint from $W^s(p_0) \bigcup W^u(p_0)$ returns to D_0 infinitely often in forward and backward time.

There is another piece of $W^u(p_0)$, near U_1, which we call U_2 and which together with a subarc of S_1 encloses a bigon strictly inside of D_0. The curve U_2 is contained in the second forward image $H^2(U_1)$. These are depicted in Figure 2. There are 12 other curves also depicted. They are pieces of $W^s(p_0)$. These curves determine rectangles, R_i, in D_0.

For space reasons, in the figure, we have left out the $R's$ and simply denoted the rectangles by their numbers. We use the number i to denote the corresponding rectangle R_i. Thus, 1 corresponds to the left most rectangle, 2 is adjacent to it on the right, etc.

The rectangles $1,2,3,4,5,6,8,9,10$ are of full-height in D_0: they are bounded above and below by pieces of the unstable curve U_1. The rectangles $7,11,12,13$ are not of full-height. Rectangle 7 is bounded above by a piece of U_2 and below by a piece of U_1. The opposite is true of rectangles $11,12,13$. They are bounded above by pieces of U_1 and below by pieces of U_2.

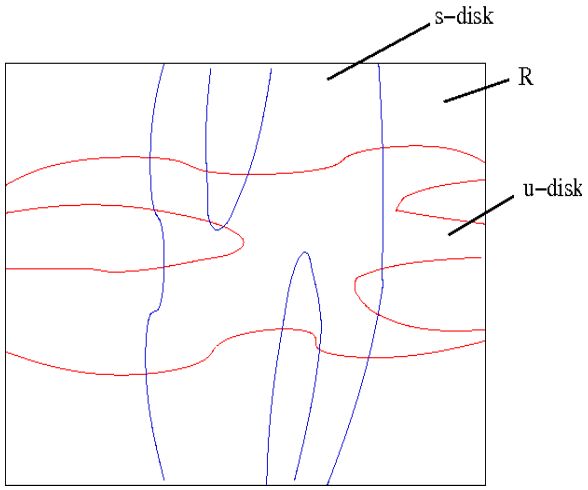

FIGURE 1. A rectangle with an $s-$disk (boundary is blue) and $u-$disk (boundary is red)

Letting r_i be the first return time of the rectangle R_i to D_0 as above, the mapping properties of the various rectangles were determined using the program COSY INFINITY [**3**]. We numerically computed (with rigorous error estimates) the image $H^{r_i}(R_i)$ of each rectangle R_i. This image will cut across certain of the rectangles R_j, in some cases more than once.

Figures 3, 4, and 5 show the rectangles R_i and their return time images (i.e.; $H^{r_i}(R_i)$). The captions describes the rectangles R_i and those which $H^{r_i}(R_i)$ meets in full-width components. Note that the boundaries of the images $H^5(R_8), H^6(R_{11})$ and $H^6(R_{13})$ are nearly tangent to the curves S_4, S_6 and S_6, respectively. To see that these images map fully across the necessary curves, we show magnified pictures of the images near the tangencies in the upper right and bottom of Figure 5. The images $H^6(R_{11}), H^6(R_{13})$ are nearly the same, so we only show the blow-ups of $H^5(R_8)$ and $H^6(R_{11})$.

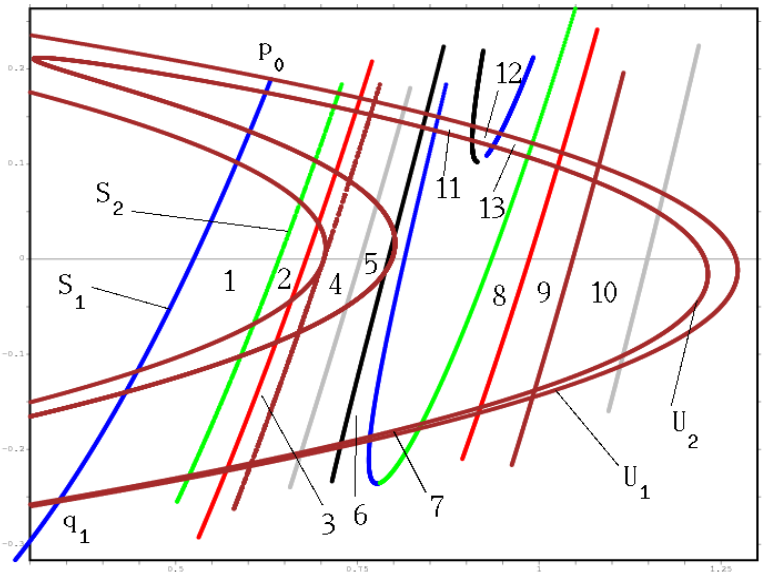

FIGURE 2. The rectangles $1,2,\ldots$ bounded by pieces of unstable and stable arcs in the standard Henon map

From the figures 3,4, and 5, it is clear that the return vector has the form

$$r = (2,2,2,2,5,5,6,5,2,2,6,7,6) \tag{11}$$

defined above.

The 13×13 matrix A is defined by the conditions $A_{ij} = k$ iff $H^{r_i}(R_i) \bigcap R_j$ consists of k full-width subrectangles.

We list this matrix in the following array. The "dots" correspond to "zeroes".

Matrix A:

$$A = \begin{pmatrix} 1 & 1 & 1 & 1 & 1 & 1 & \cdot & \cdot & \cdot & \cdot & 1 & 1 & \cdot \\ \cdot & \cdot & \cdot & \cdot & \cdot & \cdot & \cdot & 1 & \cdot & \cdot & \cdot & \cdot & 1 \\ \cdot & \cdot & \cdot & \cdot & \cdot & \cdot & \cdot & \cdot & 1 & \cdot & \cdot & \cdot & \cdot \\ \cdot & \cdot & \cdot & \cdot & \cdot & \cdot & \cdot & \cdot & \cdot & 1 & \cdot & \cdot & \cdot \\ 1 & 1 & 2 & \cdot & \cdot & \cdot & \cdot & \cdot & \cdot & \cdot & \cdot & \cdot & \cdot \\ 1 & 1 & \cdot & \cdot & \cdot & \cdot & \cdot & \cdot & \cdot & \cdot & \cdot & \cdot & \cdot \\ 2 & \cdot & \cdot & \cdot & \cdot & \cdot & \cdot & \cdot & \cdot & \cdot & \cdot & \cdot & \cdot \\ 2 & 2 & 2 & \cdot & \cdot & \cdot & \cdot & \cdot & \cdot & \cdot & \cdot & \cdot & \cdot \\ \cdot & \cdot & \cdot & \cdot & \cdot & \cdot & \cdot & \cdot & 1 & 1 & \cdot & \cdot & \cdot \\ 1 & 1 & 1 & 1 & 1 & 1 & 1 & 1 & \cdot & \cdot & \cdot & \cdot & \cdot \\ 2 & 2 & 2 & 2 & 2 & \cdot & \cdot & \cdot & \cdot & \cdot & \cdot & \cdot & \cdot \\ 2 & 2 & 2 & \cdot & \cdot & \cdot & \cdot & \cdot & \cdot & \cdot & \cdot & \cdot & \cdot \\ 2 & 2 & 2 & 2 & 2 & \cdot & \cdot & \cdot & \cdot & \cdot & \cdot & \cdot & \cdot \end{pmatrix} \tag{12}$$

The matrix B is constructed as follows. Consider the graph associated to A. It has the vertices $1,2,\ldots,13$ and A_{ij} directed edges $e_{ij,1}, e_{ij,2}, \ldots, e_{ij,A_{ij}}$ from row i to row j.

For each i, we add $r_i - 1$ new vertices, $v_{i,1}, \ldots, v_{i,r_i-1}$ with edges $i \to v_{i,1} \to v_{i,2} \to v_{i,r_i-1}$. Then, we separate the outgoing edges from i and re-attach them to the last added

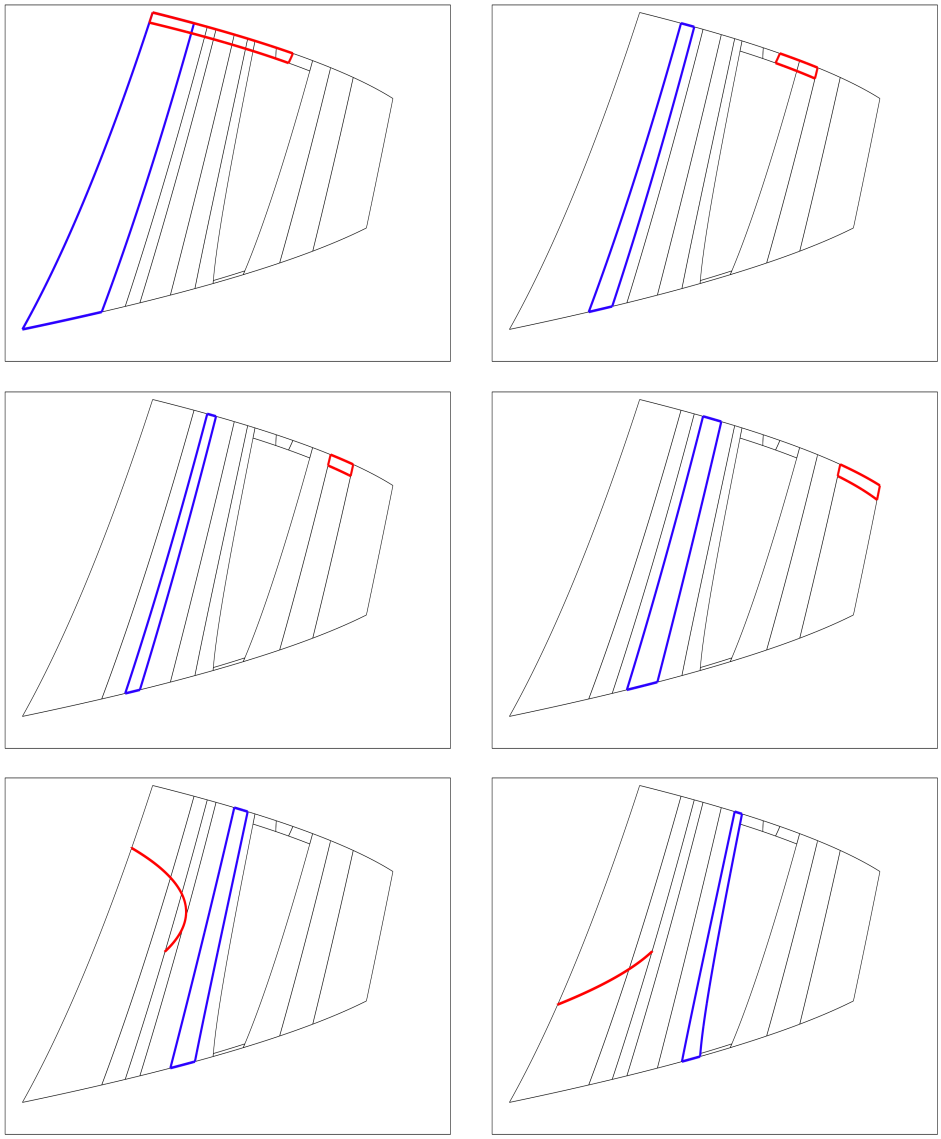

FIGURE 3. Upper left: R_1, 2nd image, $1 \to 1,2,3,4,5,6,11,12$
Upper right: R_2, 2nd image, $2 \to 13,8$
Middle left: R_3, 2nd image, $3 \to 9$
Middle right: R_4, 2nd image, $4 \to 10$
Lower left: $R5$, 5th image, $5 \to 1,2,3$ (twice)
Lower right: $R6$, 5th image, $6 \to 1,2$

vertex v_{i,r_i-1}. The matrix B is the new matrix of size $\sum r_i \times \sum r_i$ associated to this new graph. We leave the well-known details to the reader.

Computing the logarithm of the spectral radius of B, we get the lower estimate (10) above.

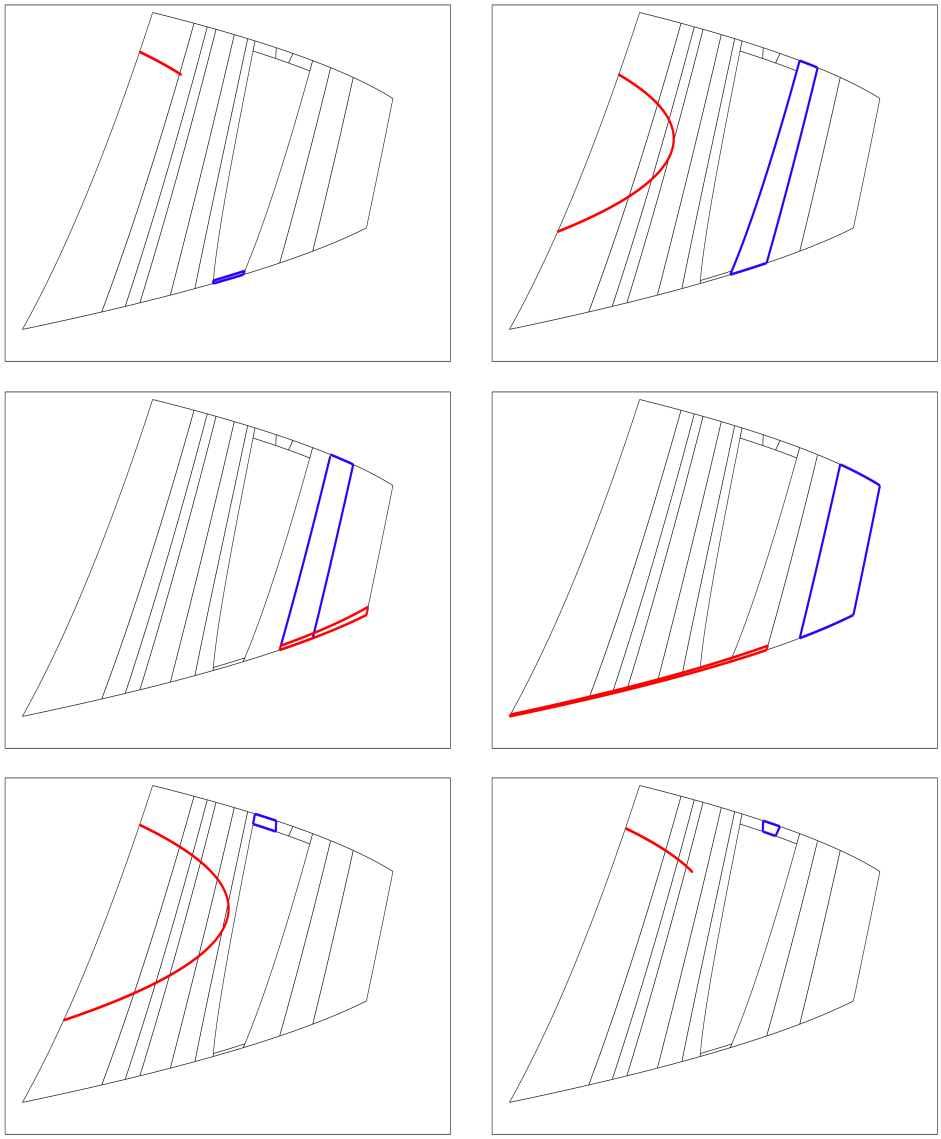

FIGURE 4. Upper left: R_7, 6th image, $7 \to 1$ (twice)
Upper right: R_8, 5th image, $8 \to 1,2,3$ (all twice)
Middle left: R_9, 2nd image, $9 \to 9,10$
Middle right: R_{10}, 2nd image, $10 \to 1,2,3,4,5,6,7,8$
Lower left: R_{11}, 6th image, $11 \to 1,2,3,4,5$ (all twice)
Lower right, R_{12}, 7th image, $12 \to 1,2,3$ (all twice)

Remark. It is interesting to compare this number with other attempts to estimate the entropy of the standard Henon map H. In [**29**] purely numerical routines based on length growth and the Takens embedding theorem are presented. In the case of the Henon map with $a = 1.4, b = 0.3$ the rough estimate for the entropy is 0.464. Zglicynski [**36**] used

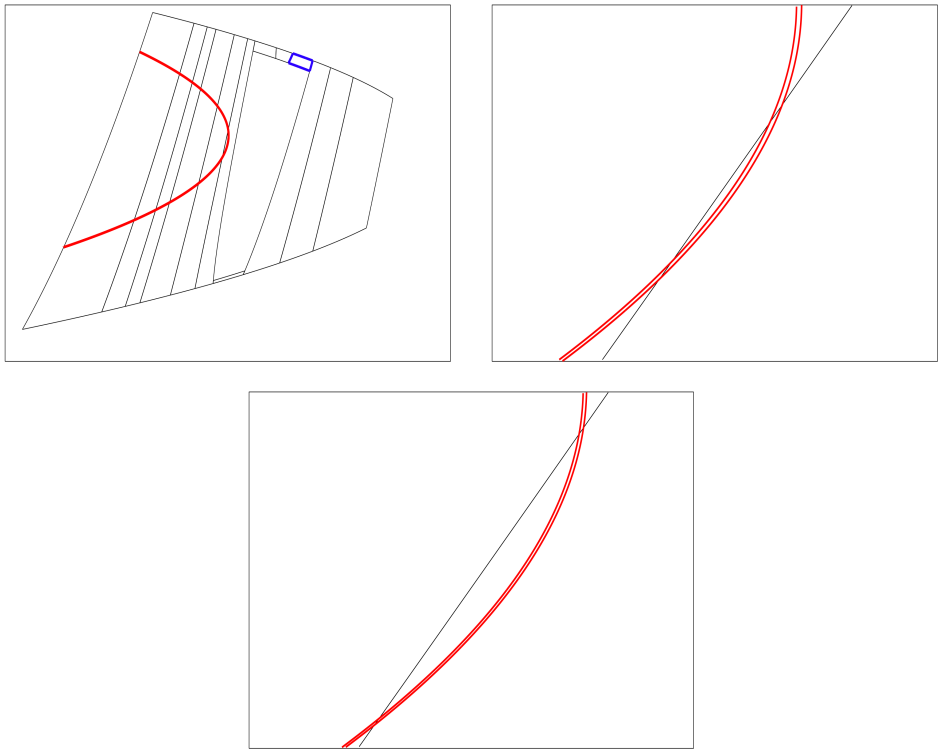

FIGURE 5. Upper left: R_{13}, 6th image, 13 → 1,2,3,4,5 (all twice)
Upper right: Blow-up of 5th image of R_8 near the tangency with S_4
Bottom: Blow-up of 6th image of R_{13} near the tangency with S_6

Conley index theory and interval arithmetic to show the existence of a horseshoe for the seventh iterate of the Hénon map, obtaining a lower entropy bound of $\frac{log2}{7}$. Subsequently, Galias and Zglicynski [**15**] used interval arithmetic to construct a SFT whose entropy is 0.33, obtaining that number as a lower bound for the entropy. More recently, Galias [**14**] obtained the lower bound 0.43.

6. Rigorous Topological Arguments in the Plane with Taylor Models

6.1. Basic Properties of Taylor Models. In the following, we develop the necessary arguments of rigorous computing to determine rigorous and tight enclosures of the stable and unstable manifolds of the Hénon map that will be used in the construction of the topological rectangles that are central to the construction of a symbolic dynamics. We begin with a brief review of some elements of Taylor model methods that are needed for the appearing topological arguments in the plane. More details about the underlying methods can be found in [**24, 22**] and references therein.

DEFINITION 6.1. ***(Taylor Model)*** *Let $D \subset \mathbb{R}^2$ be an interval box, $(x_0, y_0) \in D$, let $P : D \to \mathbb{R}$ be a polynomial of order n in two variables, and let $I \subset \mathbb{R}$ be an interval. We call the pair (P,I) a Taylor model of order n. Let $f : D \to \mathbb{R}$ be a function. We say the*

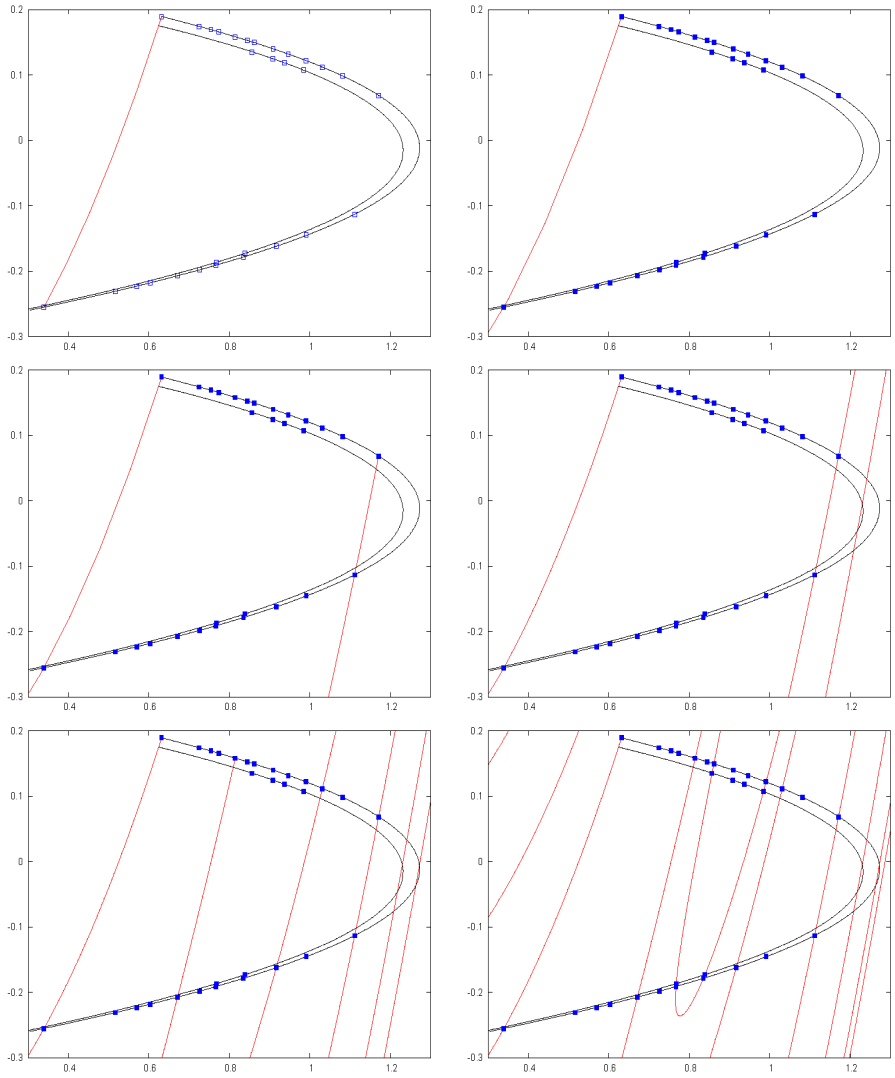

FIGURE 6. left to right, top to bottom: the pre-images $H^{-i}(S_1)$ for $0 \leq i \leq 5$ near the domain D_0.

Taylor model (P,I) is a Taylor model representation of f on D if

$$f(x,y) \in P(x-x_0, y-y_0) + I \text{ for all } (x,y) \in D.$$

Thus the polynomial P is used to "model" the behavior of the function f over the domain D. Furthermore, and importantly for our further arguments, the range of f over D

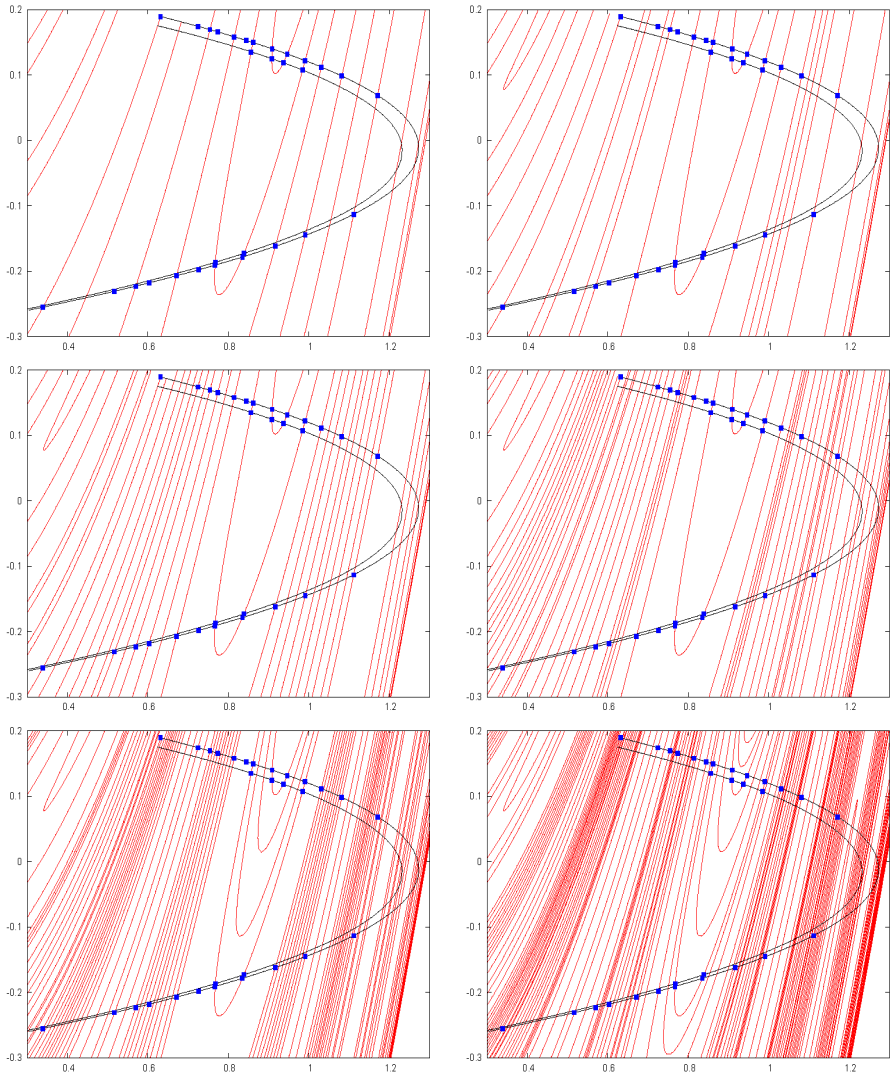

FIGURE 7. left to right, top to bottom: the pre-images $H^{-i}(S_1)$ for $6 \leq i \leq 11$ near the domain D_0.

is enclosed in the set theoretical sum of the set describing the range of P over D and the set I. Apparently, the elementary theory of Taylor's formula with remainder entails that such approximations can be quite accurate in practice, i.e. a very narrow I can be chosen. Indeed, using the notation $|A| = \sup_{x,y\in A}(|x-y|)$ for compact sets A, we have

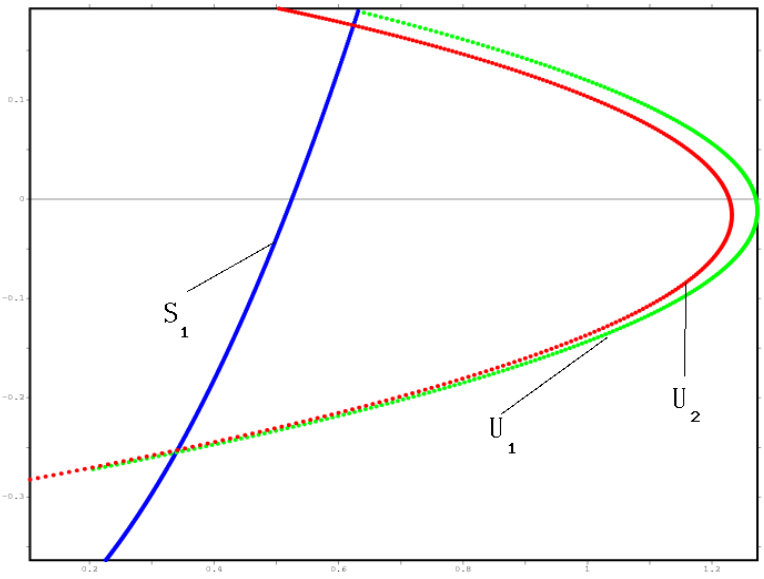

FIGURE 8. The curves S_1, U_1, U_2

REMARK 6.2. *If f is at least $(n+1)$ times continuously differentiable, then as the size $|D|$ of D decreases, so does the size $|I|$ of I, and it is possible to choose P so that we have*

$$|I| = O(|D|^{n+1}) \text{ as } |D| \to 0.$$

In fact, in practice one frequently chooses P to represent the Taylor expansion of a sufficiently smooth f around the expansion point $(x_0, y_0) \in D$.

For practical calculations, the question now is how do we arrive at a suitable P for a given f of interest. If f is given by elementary arithmetic operations, as is the case of the Hénon map to be studied, it is possible to build up Taylor models for more complicated objects from those of simpler ingredients by use of purely arithmetic operations. To this end we introduce various definitions. First, for real intervals I_1 and I_2 and the real number c, we define "interval arithmetic" $I_1 + I_2$ and $I_1 \cdot I_2$ as well as $c \cdot I_1$ in the conventional set theoretical sense. We are then ready for the following

DEFINITION 6.3. ***(Elementary Taylor Model Arithmetic)*** *Let (P_1, I_1) and (P_2, I_2) be Taylor models over the domain D with expansion point (x_0, y_0). We define addition, scalar multiplication, and multiplication of Taylor models as follows:*

$$\begin{aligned} (P_1, I_1) + (P_2, I_2) &= (P_1 + P_2, I_1 + I_2) \\ c \cdot (P, I) &= (c \cdot P, c \cdot I) \text{ for any } c \in \mathbb{R}, \text{ and} \\ (P_1, I_1) \cdot (P_2, I_2) &= (P_{1\cdot 2}, I_{1\cdot 2}) \end{aligned}$$

where $P_{1\cdot 2}$ is the part of the polynomial $P_1 \cdot P_2$ up to order n, P_e is the part of the polynomial $P_1 \cdot P_2$ of order $(n+1)$ to $2n$, and

$$I_{1\cdot 2} = I_1 \cdot I_2 + B(P_e) + B(P_1) \cdot I_2 + B(P_2) \cdot I_1$$

$B(P)$ denotes a bound for the polynomial P.

Several remarks are in order. First, we note that while there may be many choices for obtaining a "bound" B of a given $\tilde{P}$, for our purposes we merely require that the bound is at least as sharp as what is obtained by evaluating the expression $\tilde{P}(x-x_0, y-y_0)$ in interval arithmetic over the domain interval D. Furthermore, we extend the definitions to vector-valued functions in a similar way, where the corresponding Taylor model arithmetic operations happens componentwise. Finally, the question arises what these definitions on Taylor models have to do with the functions they describe. This is addressed by the following

PROPOSITION 6.4. *Let $f_{1,2} : D \subset \mathbb{R}^2 \to \mathbb{R}$ be functions. If (P_1, I_1) and (P_2, I_2) are Taylor model representations of f_1 and f_2, respectively, then $(P_1, I_1) + (P_2, I_2)$ is a Taylor model representation of $f_1 + f_2$, $(P_1, I_1) \cdot (P_2, I_2)$ is a Taylor model representation of $f_1 \cdot f_2$, and for any scalar c, the Taylor model $c \cdot (P_1, I_1)$ is a Taylor model representation of $c \cdot f_1$*

The details of the proofs rest on elementary set theoretical operations; they can be found for example in [**24, 23, 22**]. These references also contain information on more advanced operations, including common intrinsic functions and implicit functions. It is also possible to obtain rigorous enclosures of flows of ODEs [**4, 26, 25, 5**].

Thus, the proposition provides a simple mechanism to determine Taylor models for complicated functions from those comprising parts of these functions. Furthermore, the operations are particularly suitable for automated execution on a computer, since they involve only finitely many steps of elementary operations of coefficients. Based on this operation, we use the following notation:

DEFINITION 6.5. *Let F be a function comprised of finitely many operations supported in Taylor model arithmetic. Let (P, I) be a Taylor model. Then we define*

$$F((P, I))$$

to denote the Taylor model obtained by executing the individual arithmetic steps of F in Taylor model arithmetic.

Apparently, if (P, I) is a Taylor model of a function f, then the Taylor model $F((P, I))$ so obtained is a Taylor model for the function $F \circ f$.

To conclude, we note that since computers are not able to represent real numbers accurately because of finite mantissa length, in order to maintain mathematical rigor, it is important to account for these errors:

REMARK 6.6. ***(Rigorous Computer Arithmetic)*** *By careful consideration of the mathematical requirements of rounding properties of floating point computer arithmetic, it is possible to obtain rigorous Taylor model enclosures for sums, products and scalar products of functions by accounting for all round-off errors in the remainder interval I.*

We will not further dwell on this question here, although it is of course of prime importance for the claims of rigor we are making in the following statements, but rather refer to [**24, 31**] for complete details.

To conclude our introduction of the rigorous aspects of Taylor models, we note that it is clear that for complicated functions or large domains D, one single Taylor model will not be able to describe its behavior with sufficient accuracy because of the lack of or at least inefficient convergence properties of the Taylor expansion. So for this purpose it is important to split the actual domain D into a suitable finite collection of n subdomains D_i such that D lies in the union of these D_i, and apply the methods on these subdomains.

6.2. Rigorous Enclosures of Stable and Unstable Manifolds. In the following we discuss the rigorous representation of stable and unstable manifolds of the Hénon map H by Taylor models, which will be the next stepping stone to a construction of topological rectangles and the rigorous assessment of their mapping properties. Without loss of generality we restrict our discussion to the enclosure of the unstable manifold, as that of the stable manifold can be obtained by applying the same arguments to the inverse map.

We will begin by the generation of an initial enclosure of a part of the unstable manifold of the Hénon map H near the right fixed point by a two dimensional Taylor model. For the following, let $D = [-1,1]^2$, and by means of a translation, we assume that the right fixed point of H is at the origin. Since the unstable eigenvalue of $DH(0,0)$ is negative, we replace H by H^2 in the next Theorem. This insures that both components of $W^u((0,0)) \setminus \{(0,0\}$ are invariant.

THEOREM 6.7. ***(Initial Manifold Enclosure by Taylor Models)*** *Let $P = (P_1, P_2)$ be a two-dimensional bijective polynomial on $[-1,1]^2$ that satisfies $P(0,0) = (0,0)$. Let $(\tilde{P}, \tilde{I})$ be the Taylor model obtained by evaluating the map H^2 in Taylor model arithmetic as in definition (6.3), beginning with (P,I) where I is chosen as the trivial interval box $[0,0] \times [0,0]$. Thus, following the convention of definition (6.5), we have*

$$(\tilde{P}, \tilde{I}) = H^2((P,I)).$$

Let

$$R = P([-1,+1] \times [-1,+1]),\ \tilde{R} = \tilde{P}([-1,+1] \times [-1,+1]) + \tilde{I} \text{ and}$$
$$B_u = P([-1,+1] \times \{+1\}),\ B_l = P([-1,+1] \times \{-1\})$$

denote the ranges of P and $\tilde{P} + \tilde{I}$ as well as the "upper" and "lower" edges of the range $P([-1,+1] \times [-1,+1])$ of the polynomial P over $[-1,+1]^2$, respectively. Assume

$$B_u \cap \tilde{R} = \emptyset \text{ and } B_l \cap \tilde{R} = \emptyset.$$

Then the local unstable manifold through (0,0) does not leave the range R of P through B_u and B_l.

Thus the theorem provides a mechanism to generate an enclosure of the manifold, which can leave the range of P only through the "left" and "right" ends $P(\{-1\} \times [-1,+1])$ and $P(\{+1\} \times [-1,+1])$, respectively.

Proof. Let W^u_{loc} denote the connected component of $W^u((0,0))$ in R.

Assume the first crossing p of W^u_{loc} with the boundary of R is on the upper or lower boundaries B_u or B_l.

More precisely, let $[a_0, b_0]$ be a closed real interval with $a_0 < 0 < b_0$, and let $\eta : [a_0, b_0] \to \mathbf{R}^2$ be a parametrization of an arc in W^u_{loc} such that $\eta(0) = (0,0)$, $\eta(s)$ is in the interior of R for $s \in (a_0, b_0)$, and either $p = \eta(a_0)$ or $p = \eta(b_0)$.

Because p is the first crossing, the entire arc η_0 of the manifold connecting the fixed point $(0,0)$ and the point p lies in R. Consider the pre-image $\tilde{p} = H^{-2}(p)$. Since this lies in the interior of η_0, we have $\tilde{p} \in R$. Thus we have $p = H^2(\tilde{p}) \in H^2(R)$, which in turn by the properties of Taylor model arithmetic is contained in $\tilde{R}$. However, since $\tilde{R}$ is disjoint from B_u and B_l by requirement, we have a contradiction.

In practice, the usefulness of the theorem rests with the availability of a suitable choice of P. In particular, it is desirable that the range R of P be sufficiently large, and the distance between the boundaries B_u and B_l be sufficiently small. Good choices for P can be obtained by first determining a good polynomial approximation of the unstable manifold. For example, using normal form methods (see for example [**8, 2**]), it is possible to obtain

a polynomial map $\gamma\colon[-1,1]\to\mathbf{R}^2$ whose image approximates the local unstable manifold to very high orders. Using Taylor model methods, this process can even be fully automated [**2**]. Once this polynomial curve γ on $[-1,1]$ is available, one can "broaden it" by picking a vector v perpendicular to $\gamma'(0)$ and choosing

$$P(s,t)=\gamma(s)+t\cdot v$$

The length of v determines the width of the enclosure and the distance between B_u and B_l. Using this method, using conventional floating point arithmetic and γ of order 20, it is possible to obtain initial enclosures where $|R|\approx 0.1$ but $|v|\approx 10^{-15}$.

Given an initial enclosure, one can iteratively generate longer enclosures for the manifold as follows:

ALGORITHM 6.8. ***(Generation of Extended Manifold Enclosures)***

(1) *Determine an initial Taylor model enclosure of the manifold as described*
(2) *Send this enclosure through the Hénon map using Taylor model arithmetic; the resulting enclosure will again be an enclosure of the manifold*
(3) *If the resulting manifold exceeds a certain pre-specified length or the remainder bounds become too large, then split the domains of the Taylor models into suitable smaller pieces*
(4) *Iterate the procedure until enough length of manifold is generated and the desired remainder bounds are obtained*

6.3. Rectangles and Their Mapping Properties. In the following we will use parts of the unstable and stable manifolds to form curvilinear rectangles. Using images of rigorous enclosures of stable and unstable manifold obtained with Taylor model arithmetic, and the well-known invariance of stable and unstable manifold under forward or backward iteration, we will prove crossing properties of these rectangles under suitable iterations of the Hénon map H. Recall the definitions of the unstable arcs U_1 and U_2 defined following the statement of Theorem 5.1.

DEFINITION 6.9. ***(Stable Rectangle Boundaries)*** *Let S_1 be the interval in the stable manifold connecting the fixed point p_0 to the homoclinic point q_1 and consider the 11th pre-image $S=H^{-11}S_1$. We define additional subarcs S_2 through S_{13} of S as shown in figure 2. The arcs $S_1,\dots,S_{11}$ in Figure 2 actually extend slightly above and below the domain D_0. We crop them so that they terminate in U_1. We crop the subarcs S_{12} and S_{13} so that their endpoints lie in U_1 or U_2.*

To avoid ambiguity and help in identification, we list the number of the iterate of H^{-1} at which each of S_1 through S_{13} first appear. With one exception, this number is much smaller than 11, leading to easy identification of the corresponding pieces.

$$\begin{array}{lllll} S_1:0 & S_2:8 & S_3:6 & S_4:8 & \\ S_5:4 & S_6:11 & S_7:5 & S_8:5 & \\ S_9:4 & S_{10}:6 & S_{11}:2 & S_{12}:6 & S_{13}:6 \end{array}$$

The verification of the inverse iterates at which the various $S_i's$ first appear can be seen in Figures 6 and 7. The figures contain the boundary points of the rectanges R_i, the arcs U_1,U_2 and the indicated pre-images of S_1.

DEFINITION 6.10. ***(Curvilinear Rectangles)*** *We define the rectangles R_1 through R_{13}, each of which is formed by stable arcs and two unstable arcs as shown in figure 2. The unstable arcs are in U_1 or U_2 (which is in the second image of U_1), while the stable arcs in the eleventh pre-image of S_1.*

For keep further discussion transparent, we observe the following.

PROPOSITION 6.11. *Let n_l and n_r denote the pre-iterate of S_1 under which the left and right boundaries of a rectangle under consideration first appear. Summarizing from the definitions of the stable rectangle boundaries S_1 through S_{13} and the rectangles R_1 through R_{13}, we have the following result.*

Rectangle	n_l	n_r	*Rectangle*	n_l	n_r
R_1	0	8	R_8	5	4
R_2	8	6	R_9	4	6
R_3	6	8	R_{10}	6	3
R_4	8	4	R_{11}	5	6
R_5	4	11	R_{12}	6	6
R_6	11	5	R_{13}	6	5
R_7	5	5			

THEOREM 6.12. *The rectangles R_1 through R_{13} satisfy the following mapping properties:*

$H^2(R_1)$ crosses $R_1, R_2, R_3, R_4, R_5, R_6, R_{11}$ and R_{12}.
$H^2(R_2)$ crosses R_{13} and R_8.
$H^2(R_3)$ crosses R_9.
$H^2(R_4)$ crosses R_{10}.
$H^5(R_5)$ crosses R_1, R_2, R_3; the crossing of R_3 is a double crossing.
$H^5(R_6)$ crosses R_1 and R_2.
$H^6(R_7)$ crosses R_1; the crossing is a double crossing.
$H^5(R_8)$ crosses R_1, R_2 and R_3. All crossings are double crossings.
$H^2(R_9)$ crosses R_9 and R_{10}.
$H^2(R_{10})$ crosses R_1, R_2, R_3, R_4, R_5, R_6, R_7 and R_8.
$H^6(R_{11})$ crosses R_1, R_2, R_3, R_4 and R_5. All crossings are double crossings.
$H^7(R_{12})$ crosses R_1, R_2 and R_3. All crossings are double crossings.
$H^6(R_{13})$ crosses R_1, R_2, R_3, R_4 and R_5. All crossings are double crossings.

The proofs for each of the cases are very similar. They consist of visually inspecting the pictures showing the mapping properties, which because of the use of rigorous Taylor model arguments have an accuracy well below printer resolution. To decide whether edges lie on top of each other, which can obviously not be decided from a printed image, we employ the knowledge of the pre-iterate of S_1 where the edges of the rectangles under consideration first appear. Since the branches of these pre-images are well separated in the printed image, the mapping properties of stable edges can be uniquely and rigorously decided. Specifically, we argue as follows.

Proof.

R_1 : Because the upper boundary of R_1 lies on the unstable manifold, so does its second image. From the picture we see that this does not extend outside U_1, and in fact, the union of the upper edges of $R_1, ..., R_6, R_{11}, R_{12}$ is the upper edge of $H^2(R_1)$. The lower edge of $H^2(R_1)$ lies within the fundamental domain and hence does not cross the lower edges of $R_1, ..., R_6$. It also does not cross the lower edges of R_{11} and R_{12}, but rather coincides with them, since these lower edges by definition are in the second image of U_1. So we see from the picture that it is clear that $H^2(R_1)$ crosses $R_2, ..., R_6$ and R_{11}. To see that $H^2(R_1)$ also crosses R_1, observe that according to proposition 6.11, the left edge of R_1 lies in S_1, and so does its second image; hence the left edge of $H^2(R_1)$ is a subset of the left edge of R_1. To see that $H^2(R_1)$ also crosses R_{12}, we first observe that by proposition 6.11, the right

stable edge of R_1 first appears in the eighth pre-iterate of S_1. Thus the right edge of $H^2(R_1)$ first appears in the sixth pre-iterate of S_1. According to figure 7, the only part of the sixth pre-image of the stable arc that is near the right edge of $H^2(R_1)$ to the resolution of the picture is S_{13}, which contains the right edge of R_{12}. Thus the right edge of $H^2(R_1)$ and R_{12} agree, and we have shown that $H^2(R_1)$ crosses R_{12}.

R_2 : For the upper and lower unstable boundary of $H^2(R_2)$ we argue as in the case of R_1. Furthermore, since the left edge of R_2 first appears in the eighth pre-image of S_1, $H^2(R_2)$ first appears in its sixth pre-image. As seen in figure 7, the only part of this sixth pre-image that lies near the left edge of $H^2(R_2)$ to printer resolution is indeed the line S_{13}, which is used to form the left edge of R_{13}. Thus the left edge of R_{13} and the left edge of $H^2(R_2)$ coincide, and we have shown that $H^2(R_2)$ crosses R_{13}. In a conceptually identical way, we see that the right edge of $H^2(R_2)$ is a subset of the right edge of R_{10}, so that $H^2(R_2)$ is shown to cross R_{10}.

R_3 : The argument is similar to above; note that according to proposition 6.11, the left and right stable edges of R_3 lie in the sixth and eighth pre-image of the fundamental stable arc, respectively, so that $H^2(R_3)$ must lie in the fourth and sixth such pre-image. Since the picture of the pre-images is accurate to printer resolution, the only possibility is for the left and right edges of $H^2(R_3)$ to be subsets of the left and right pre-images of R_9, which by definition are taken from the fourth and sixth pre-image of the stable fundamental arc.

R_4 : The argument is conceptually identical to that of R_3.

R_5 : From the picture it is clear that the $H^5(R_5)$ crosses R_2. Considering that the left edge of R_5 appear in the fourth pre-image of the S_1, its fifth image lies in S_1, which forms the left boundary of R_1. Thus $H^5(R_5)$ crosses R_1. Since the right edge of R_5 lies in the eleventh pre-image of the S_1, so the right edge of $H^5(R_5)$ lies in the sixth pre-image of the S_1. The only part of that sixth pre-image that coincides with the right edge of $H^5(R_5)$ to printer resolution is S_3, so the right edge must lie in S_3, and thus in the left boundary of R_3. Finally we observe that both upper and lower edge of $H^5(R_5)$ extend to the right of the right edge of R_3, which is seen by magnification in figure 5. Again the magnified picture is accurate to printer resolution since the accuracy of the Taylor model enclosures lie below it. Thus $H^5(R_5)$ crosses R_3 twice.

R_6 : The argument is conceptually identical to that of R_3 and R_4.

R_7 : According to proposition 6.11, both edges of R_7 lie in the fifth pre-image of S_1. Thus their sixth images, and hence both the left and right edges of $H^6(R_7)$, lie in the left edge of R_1. Furthermore, a close visual inspection of both the upper and lower boundaries of $H^6(R_7)$ shows that they extend to the right of the right boundary of R_1 (in fact they nearly fold back upon themselves). Thus $H^6(R_7)$ crosses R_1 twice.

R_8 : Similar to R_5, we observe that both edges of $H^5(R_8)$ lie on S_1. Furthermore, a magnified inspection shows that both upper and lower edges of $H^5(R_8)$ extend beyond the right edge of R_3. Thus we conclude that $H^5(R_8)$ crosses each of R_1, R_2 and R_3 twice.

R_9 : The argument is conceptually identical to that of R_2.

R_{10} : As in R_1.

R_{11} : As in R_8, except no magnification is necessary.

R_{12} : As in R_7.

R_{13} : As in $R_{11}$and R_8.

7. An alternate numerical description of the rectangles R_i and their properties

In this section, we describe the numerical calculations which we used to produce the rectangles in Figure 2. These calculations were done with numerical techniques suggested

by Theorem 4.1, and they provide alternative numerical constructions to those described in the preceding section. As we mentioned above, the rectangles and mapping properties in Figures 3, 4, and 5 were done with the program COSY INFINITY. The latter program, together with the Taylor Model methods discussed in the preceding section provide the methods used to prove the theorems below. Nevertheless, the use of the two different methods provide independent means of verifying the locations of the indicated rectangles and their mapping properties.

Let $\lambda_1 \sim -1.92$, $\lambda_2 \sim \lambda_s = .15$ be the two eigenvalues of $DH(p_0)$. It is easy to check that there are eigenvectors v_1, v_2 associated to λ_1, λ_2, respectively, of the form

$$v_1 = \begin{pmatrix} 1 \\ -\lambda_2 \end{pmatrix},\ v_2 = \begin{pmatrix} 1 \\ -\lambda_1 \end{pmatrix}.$$

Let $W^u(p_0)$, $W^s(p_0)$ denote, respectively, the unstable and stable manifolds of p_0. From Theorem 6, we can parametrize those manifolds as in Theorem 6 with the curves $\gamma^u(t), \gamma^s(t)$ so that $\gamma^u(0) = p_0 = \gamma^s(0)$, $\frac{d}{dt}\gamma^u(0) = v_1$, $\frac{d}{dt}\gamma^s(0) = v_2$.

Given a positive integer n, we also have the approximating curves

$$\gamma^u_n(t) = H^n(p_0 + \lambda_1^{-n} t v_1),$$

and

$$\gamma^s_n(t) = H^{-n}(p_0 + \lambda_s^n t v_2),$$

which, according to Theorem 6, converge to $\gamma^u(t)$, $\gamma^s(t)$, respectively, as $n \to \infty$.

For real numbers $r < s$, let

$$ws(r,s) = \{\gamma^s(t) : t \in (r,s)\},\ \ wu(r,s) = \{\gamma^u(t) : t \in (r,s)\},$$

$$ws_n(r,s) = \{\gamma^s_n(t) : t \in (r,s)\},\ \ wu_n(r,s) = \{\gamma^u_n(t) : t \in (r,s)\}.$$

denote the images of the restrictions of the functions γ^s, $\gamma^u, \gamma^u_n, \gamma^s_n$ to the interval (r,s), respectively.

In Figure 8 we used γ^u_{10} and γ^s_{10} as approximations to the curves γ^u and γ^s. Thus, when we say that $wu(0,5.5)$ is described in a figure, we actually represent it by $wu_{10}(0,5.5)$. Of course, one could get better approximations to the stable and unstable manifolds by choosing higher integers n and computing $ws_n(r,x), wu_n(r,s)$. As n gets larger, floating point issues start to affect the computations. We have had good results, using standard double precision, for $ws_{14}(r,s)$ and $wu_{40}(r,s)$ For n higher, it may be necessary to use higher precision arithmetic.

The intervals U_i, S_i to be defined below are actually slightly larger than those with the same names which were defined in section 6. The latter intervals were *cut off* at the homoclinic intersections.

Consider the real intervals $(0,5.5), (12.2,20)$ and $(-.5,0)$ and associated image intervals

$$U_1 \stackrel{\text{def}}{=} wu(0,5.5),\ U_2 \stackrel{\text{def}}{=} wu(12.2,20),\ S_1 \stackrel{\text{def}}{=} ws(-0.5,0)$$

as in Figure 8. The curve S_1 goes monotonically up toward the fixed point p_0. The curve $U_1 = wu(0,5.5)$ starts toward the right of p_0, moving downward, passing through the homoclinic point q_1. Increasing the parameter $t \in (0,20)$ in the curve $wu(0,20)$, we meet the curve curve $U_2 = wu(12.2,20)$ which winds back and forth crossing S_1 in two more

homoclinic points q_2 and q_3. Let $t_1 < t_2 < t_3 \in (0,20)$ and $s_1 < s_2 < s_3 \in (-.5,0)$ be the parameters such that $q_i = \gamma^u(t_i) = \gamma^s(s_i)$ for $i = 1,2,3$.

The set $\eta_0 \stackrel{\text{def}}{=} \{p_0\} \bigcup wu(0,t_1) \bigcup \{q_1\} \bigcup ws(s_1,0)$ is a Jordan curve. Let D_0 denote the bounded region of the complement of η_0. We call D_0 the *primary region* for H. Every bounded orbit of H visits $Closure(D_0)$.

Let us define some additional specific intervals I_j, S_j with $2 \le j \le 13$ in $W^s(p_0)$, and put them, together with S_1, U_1 in the table below.

Let $V^+ = \{y > 0\}$ and $V^- = \{y < 0\}$ denote the upper and lower half-planes in $\mathbf{R}^2$.

The intervals S_j, $1 \le j \le 11$ will each have homoclinic intersections with U_1, at least one in V^+ and at least one in V^-. [1] The intervals S_{12}, S_{13} will be completely contained in V^+.

We begin by defining I_j and S_j for $2 \le j \le 11, j \ne 6$ as in the next table.

$$
\begin{array}{lll}
I_2 = & ws(-.2384265, -.2384254) & S_2 = H^{-8} I_2 \\
I_3 = & ws(-.350785, -.350773) & S_3 = H^{-6} I_3 \\
I_4 = & ws(-.3509603, -.3509598) & S_4 = H^{-8} I_4 \\
I_5 = & ws(-0.3537, -0.35309) & S_5 = H^{-4} I_5 \\
I_7 = & ws(-.21915, -.21899) & S_7 = H^{-5} I_7 \\
I_8 = & ws(-.21928, -.21915) & S_8 = H^{-5} I_8 \\
I_9 = & ws(-.351, -.3507) & S_9 = H^{-4} I_9 \\
I_{10} = & ws(-.350962, -.350954) & S_{10} = H^{-6} I_{10} \\
I_{11} = & ws(-.354, -.3505) & S_{11} = H^{-2} I_{11} \\
I_{12} = & ws(-.238434, -.2384285) & S_{12} = H^{-6} I_{12} \\
I_{13} = & ws(-.238427, -.238423) & S_{13} = H^{-6} I_{13}
\end{array} \tag{13}
$$

For I_6 and S_6, we first consider the points

$$p_{6a} = (0.341125816447222, -0.252568347231336),$$

and

$$p_{6b} = (.3411258214153245, -.2525683416553848).$$

Then, we set I_6 to be the line segment

$$\eta_6(t) = \{(1-t)p_{6a} + t p_{6b} : t \in [0,1]\},$$

and set $S_6 = H^{-11} I_6$.

The intervals S_i and U_1, U_2 are shown in Figure 2.

These intervals determine rectangles R_i, $1 \le i \le 13$ which are defined as follows.

(1) The rectangles R_i for $1 \le i \le 6$ and $8 \le i \le 10$ are bounded on the left by S_i, on the right by S_{i+1} and above and below by pieces of U_1,
(2) the rectangle R_{11} is bounded above by a part of U_1, below by a part of U_2, bounded on the left by a part of S_7, and on the right by a part of S_{11},
(3) the rectangle R_{12} is bounded above by a part of U_1, below by a part of U_2, bounded on the left by a part of S_{11}, and on the right by a part of S_{12},
(4) the rectangle R_{13} is bounded above by a part of U_1, below by a part of U_2, bounded on the left by a part of S_{12}, and on the right by a part of S_8,

[1] It seems from the computer images that, in fact, S_i will meet U_1 in exactly two points, but we have not yet proved that.

(5) the rectangle R_7 is bounded above by a part of U_2, below by a part of U_1, bounded on the left by a part of S_7, and on the right by a part of S_8, and

Now, we state two theorems giving the properties of the boundary curves of the rectangles we have defined which are necessary for the entropy estimate (10). The proof of Theorem 7.1 relies on the methods sketched in section 6. The details will be given elsewhere. Theorem 7.2 is essentially a restatement of Theorem 6.12.

Recall that, given a point $x \in \mathbf{R}^2$ and a compact subset $E \subset \mathbf{R}^2$, we define the *distance* from x to E by the formula

$$dist(x,E) = \min(d(x,y) : y \in E).$$

For $\varepsilon > 0$, the $\varepsilon-$neighborhood of E , denoted $B_\varepsilon(E)$,
is the set

$$B_\varepsilon(E) = \{x \in \mathbf{R}^2 : dist(x,E) < \varepsilon\}$$

If E is compact and connected, then an $\varepsilon-$enclosure of E is a compact connected neighborhood of E which is contained in $B_\varepsilon(E)$.

We will use the notation $\mathcal{N}_\varepsilon(E)$ to denote various, possibly different $\varepsilon-$enclosures of sets E.

Recall that D_0 is the region whose boundary is the closure of the union $S_1 \bigcup U_1$.

Let D_1 be the bigon inside D_0 bounded by pieces of U_2 and S_1.

Set $\varepsilon_0 = 0.001$, and define the subsets

$$V_0^+ = V^+ \setminus B_{2\varepsilon_0}(D_0),$$

$$V_0^- = V^- \setminus B_{2\varepsilon_0}(D_0),$$

$$V_1^+ = V^+ \bigcap B_{2\varepsilon_0}(\mathbf{R}^2 \setminus D_0),$$

and

$$V_1^- = V^- \bigcap B_{2\varepsilon_0}(\mathbf{R}^2 \setminus D_0).$$

Since $U_2 \subset B_{\frac{\varepsilon_0}{2}} U_1$ we have that both V_1^+ and V_1^- lie in D_1.

THEOREM 7.1. *With the above definitions, there exist ε_0-enclosures $\mathcal{N}_{\varepsilon_0}(S_i)$ for $1 \leq i \leq 13$ with the following properties.*

(1) *For $1 \leq i \leq 13$, the ε_0-enclosures $\{\mathcal{N}_{\varepsilon_0}(S_i)\}$ form a disjoint collection of sets.*
(2) *The enclosure $\mathcal{N}_{\varepsilon_0}(S_1)$ meets both of the sets V_0^+ and V_0^-, and, for $2 \leq i \leq 11$, each of the enclosures $\mathcal{N}_{\varepsilon_0}(S_i)$ has a non-empty intersection with each of the four sets $V_0^+, V_1^+, V_0^-, V_1^-$. In adddition, there is an increasing sequence of real numbers $x_1 < x_2 < \ldots, x_{11}$ such that for each i, the point p_i defined by $p_i = (x_i, 0)$ lies in the curve S_i.*
(3) *For $i = 12,\ 13$, $\mathcal{N}_{\varepsilon_0}(S_i) \subset V^+$, and both enclosures $\mathcal{N}_{\varepsilon_0}(S_i)$ have non-empty intersections with each of the sets V_0^+ and V_1^+.*

THEOREM 7.2. *Let*

$$r = (r_1, r_2, \ldots, r_{14}) = (2,2,2,2,5,5,6,5,2,2,6,7,6)$$

be the vector of return times defined in (11). There is a 13×13 *matrix A having the form in (12) such that* $A_{i,j} = k$ *if and only if* $H^{r_i}R_i \bigcap R_j$ *contains k disjoint u−disks in* R_j *and* $R_i \bigcap H^{-r_i}(R_j)$ *contains k disjoint s−disks.*

References

[1] N. J. Balmsforth, E. A. Spiegel, and C. Tresser. The topological entropy of one-dimensional maps: approximations and bounds. *Phys. Rev. Lett.*, 80:80–83, 1994.

[2] M. Berz. *Modern Map Methods in Particle Beam Physics*. Academic Press, San Diego, 1999. Also available at http://bt.pa.msu.edu/pub.

[3] M. Berz and K. Makino. COSY INFINITY. `http://www.cosyinfinity.org` .

[4] M. Berz and K. Makino. Verified integration of ODEs and flows using differential algebraic methods on high-order Taylor models. *Reliable Computing*, 4(4):361–369, 1998.

[5] M. Berz and K. Makino. Suppression of the wrapping effect by Taylor model- based verified integrators: Long-term stabilization by shrink wrapping. *International Journal of Differential Equations and Applications*, 10, 2005.

[6] L. Block, J. Keesling, S. Li, and K. Peterson. An improved algorithm for computing topological entropy. *J. Stat. Phys.*, 55:929–939, 1989.

[7] K. Burns and H. Weiss. A geometric criterion for positive topological entropy. *Comm. Math. Phys*, 172(1):95–118, 1995.

[8] X. Cabré, E. Fontich, and R. de la Llave. The parametrization method for invariant manifolds i: manifolds associated to non-resonant subspaces. *Indiana Univ. Math J.*, 52:283–328, 2003.

[9] X. Cabré, E. Fontich, and R. de la Llave. The parametrization method for invariant manifolds iii: overview and applications. *J. Diff. Eq*, 218:444–515, 2005.

[10] P. Collins. Dynamics of surface diffeomorphisms relative to homoclinic and heteroclinic orbits. *Dynamical Systems*, 19:1–39, 2004.

[11] P. Collins. Entropy-minimizing modesl of surface diffeomorphisms relative to homoclinic and heteroclinic orbits. *Dynamical Systems*, 20(4):369–400, 2005.

[12] S. Day, R. Frongillo, and R. Trevino. Algorithms for rigorous entropy bounds and symbolic dynamics. *preprint,www.math.wm.edu/∼day/topent.pdf*, 2007.

[13] V Franceschini and L. Russo. Stable and unstable manifolds of the Hénon mapping. *Jour. Stat. Phys.*, 25(4):757–769, 1981.

[14] Z. Galias. Obtaining rigorous bounds for topological entropy for discrete time dynamical systems. In *Proc. Int. Symposium on Nonlinear Theory and its Applications, NOLTA'02*, pages 619–622, Xi'an, PRC, 2002.

[15] Z. Galias and P. Zgliczynski. Abundance of homoclinic and heteroclinic orbits and rigorous bounds for the topological entropy of the Hénon map. *Nonlinearity*, 14:909–932, 2001.

[16] B. Hasselblatt and A. Katok. *Introduction to the Modern Theory of Dynamical Systems*, volume 54 of *Encyclopedia of Mathematics and Its Applications*. Cambridge University Press, 1995.

[17] M. Hénon. A two-dimensional mapping with a strange attractor. *Commun. Math. Phys.*, 50:69–77, 1976.

[18] D. Hobson. An efficient method for computing invariant manifolds of planar maps. *J. Comput. Phys.*, 104(14), 1993.

[19] J. Hubbard. Parametrizing unstable and very unstable manifolds. *Moscow Mathmatical Journal*, 5(1):105–124, 2005.

[20] A. Katok. Lyapunov exponents, entropy and periodic orbits for diffeomorphisms. *Publ. Math. IHES*, 51:137–173, 1980.

[21] B. Krauskopf and H. Osinge. Growing 1d and quasi-2d unstable manifolds of maps. *J. Comput. Phys.*, 146:404–419, 1998.

[22] K. Makino. *Rigorous Analysis of Nonlinear Motion in Particle Accelerators*. PhD thesis, Michigan State University, East Lansing, Michigan, USA, 1998. Also MSUCL-1093.

[23] K. Makino and M. Berz. Remainder differential algebras and their applications. In M. Berz, C. Bischof, G. Corliss, and A. Griewank, editors, *Computational Differentiation: Techniques, Applications, and Tools*, pages 63–74, Philadelphia, 1996. SIAM.

[24] K. Makino and M. Berz. Taylor models and other validated functional inclusion methods. *International Journal of Pure and Applied Mathematics*, 6,3:239–316, 2003.

[25] K. Makino and M. Berz. Suppression of the wrapping effect by Taylor model- based verified integrators: Long-term stabilization by preconditioning. *International Journal of Differential Equations and Applications*, 10,4:253–384, 2005.

[26] K. Makino and M. Berz. Suppression of the wrapping effect by Taylor model- based verified integrators: The single step. *International Journal of Pure and Applied Mathematics*, 36,2:175–187, 2006.
[27] S. Newhouse. Entropy and volume. *Ergodic Theory and Dynam. Sys.*, 8:283–299, 1988.
[28] S. Newhouse. Continuity properties of entropy. *Ann. Math.*, 129:215–235, 1989.
[29] S. Newhouse and T. Pignataro. On the estimation of topological entropy. *Jour. Stat. Phys*, 72(5-6):1331–1351, 1993.
[30] A. Radulescu. Computing topological entropy in a space of quartic polynomials. *Jour. Stat. Phys.*, page to appear.
[31] N. Revol, K. Makino, and M. Berz. Taylor models and floating-point arithmetic: Proof that arithmetic operations are validated in COSY. *Journal of Logic and Algebraic Programming*, 64/1:135–154, 2004.
[32] P. Walters. *An introduction to ergodic theory*. Springer–Verlag, 1982.
[33] Y. Yomdin. Volume growth and entropy. *Israel J. Math.*, 57:285–300, 1987.
[34] Y. Yomdin. Local complexity growth for iterations of real analytic mappings and semicontinuity moduli of the entropy. *Ergodic Theory and Dynamical Systems*, 11:583–602, 1991.
[35] Z. You, E. Kostelich, and James A. Yorke. Calculating stable and unstable manifolds. *International Jour. of Bifurcation and Chaos*, 1(3):605–623, 1991.
[36] P. Zgliczynski. Computer assisted proof of the horseshoe dynamics in the Hénon map. *Random Computational Dynamics*, 5(1):1–17, 1997.